Theor Chem Acc (2009) 124:139–150
DOI 10.1007/s00214-009-0592-2

REGULAR ARTICLE

Ab initio and ABEEM/MM fluctuating charge model studies of dimethyl phosphate anion in a microhydrated environment

Fang-Fang Wang · Dong-Xia Zhao · Li-Dong Gong

Received: 18 January 2009 / Accepted: 15 May 2009 / Published online: 3 June 2009

Abstract Dimethyl phosphate (DMP) anion has been used extensively as a model compound to simulate the properties of phosphate group. A 35-point DMP anion potential model is constructed based on the atom-bond electronegativity equalization fluctuating charge molecular force field (ABEEM/MM), and it is employed to study the properties of gas-phase DMP anion and DMP-$(H_2O)_n$ ($n = 1$–3) clusters. The ABEEM/MM model reproduces well the properties obtained by available experiments and QM calculations, including charge distributions, geometries, and conformational energies of gas-phase DMP-water complexes. Furthermore, molecular dynamics simulation on the DMP anion in aqueous solution based on the ABEEM/MM shows that a remarkable first hydration shell around the nonesterified oxygen atom of DMP anion is formed with a coordination number of 5.2. It is also found that two hydrogen atoms of one water molecule form two hydrogen bonds with two nonesterified oxygen atoms of DMP anion simultaneously. This work could be used as a starting point for us to establish the ABEEM/MM nucleic acid force field.

Keywords ABEEM/MM · Fluctuating charge force field · Ab initio calculation · Dimethyl phosphate anion · Molecular dynamics simulation

Electronic supplementary material The online version of this article (doi:10.1007/s00214-009-0592-2) contains supplementary material, which is available to authorized users.

F.-F. Wang · D.-X. Zhao · L.-D. Gong (✉)
School of Chemistry and Chemical Engineering, Liaoning Normal University, 116029 Dalian, People's Republic of China
e-mail: gongjw@lnnu.edu.cn

1 Introduction

Dimethyl phosphate (DMP) anion represents the smallest realistic model systems of the phosphodiester linkage in the highly charged backbone of nucleic acids. It has been used extensively as a model compound to simulate the properties of phosphate group [1, 2]. Furthermore, DMP is a vital first step toward developing and validating of a new nucleic acid force field. Three conformations of DMP anion, shown in Fig. 1 in the gauche-gauche (gg), gauche-trans (gt), and trans–trans (tt) conformations, are found to be significant for the phosphodiester torsions from both experimental and theoretical studies [3, 4].

There have been many theoretical studies on DMP anion [5–19]. For example, Landin et al. [7] have investigated the DMP anion at the Hartree-Fock level using the 3-21G, 3-21G(*), 6-31G*, and 6-31+G* basis set in 1995. Florián et al. [9] have carried out several quantum chemical calculations at HF/3-21G(*), HF/6-31G*, MP2/6-31+G*, and B3LYP/6-31G* levels in 1996, and they found that the best results were obtained by using the B3LYP gradient corrected density functional. Very recently, Petrov et al. [18] performed calculations at the B3LYP/6-31G** level of theory within the framework of the COSMO polarized continuum model. Kuo and Tobias [15] reported an ab initio molecular dynamics simulation study of sodium DMP in aqueous solution. However, the ab initio molecular dynamics simulation was only possible to simulate small and medium-size molecules and their complexes.

Computer simulations based on molecular mechanics (MM) are now an informative source for investigating dynamical structures and properties of biomolecules [20–24]. Up to date, a majority part of the potential functions for studying nucleic acid systems employ the fixed-charge potential models [25–31]. Shaik et al. [29] have

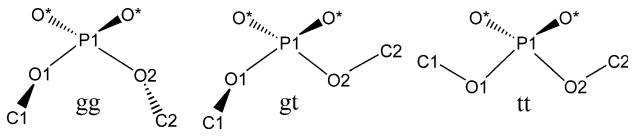

Fig. 1 Graphical representation of DMP anion in gg, gt, and tt conformations

scrutinized the performance of popular point charge models such as AMBER, CHARMM, OPLS, MMFF, TAFF, and TIP4P. The crucial problem in many force fields arises from the calculation of Coulomb interactions with the fixed charges that neglect all mutual polarizations and charge-transfer effects. Previous studies [17] showed that empirical force field significantly underestimated the total interaction energies of DMP complexes, due to an inaccurate description of the electrostatic interaction between monomer at close distances. The atomic charges, however, should vary with the environmental field and the geometry of the system. There has been steady interest since the 1970s in the development and use of polarizable force fields [32]. Some electrostatic protocols including polarization effects have been widely developed in the past few years [32–51]. Furthermore, some fluctuating charge models based on the electronegativity equalization principle (see reference [52] and references therein) were proposed to overcome the limitation of the fixed charge model. Based on the atom-bond electronegativity equalization method (ABEEM) [53–56], Yang et al. have developed the ABEEM/MM fluctuating charge model, which has been applied successfully to the water system [57–62], organic molecules and peptides [52, 63–65]. It has also been used to study the solvation of atomic ion, such as alkaline cation, alkaline-earth cation, halogen anion and so on [59–61].

In the present paper, we investigated the properties of isolated DMP anion, DMP-water clusters and DMP anion in aqueous solution with quantum mechanics (QM) methods and/or the newly constructed ABEEM/MM model. This is the first time for ABEEM/MM to cover DNA fragment, and this work will be used as a starting point for us to develop a new nucleic acid force field. The remainder of this article is organized as follows. Section 2 describes the theoretical model and computational details. Section 3 gives the results and discussion of the system concerned. Finally, a conclusion is presented in Sect. 4.

2 Methods

The potential energy function in ABEEM/MM can be expressed as follows:

$$\begin{aligned} E_{\mathrm{ABEEM/MM}} = & \sum_{\text{bonds}} k_r (r - r_{eq})^2 + \sum_{\text{angles}} k_\theta (\theta - \theta_{\mathrm{eq}})^2 \\ & + \sum_{\text{torsions}} \left\{ \frac{v_1}{2}[1 + \cos(\phi)] + \frac{v_2}{2}[1 - \cos(2\phi)] \right. \\ & \left. + \frac{v_3}{2}[1 + \cos(3\phi)] \right\} \\ & + \sum_{i(j} \left[k_{ij} \frac{q_i q_j e^2}{R_{ij}} + 4 f_{ij} \varepsilon_{ij} \left(\frac{\sigma_{ij}^{12}}{R_{ij}^{12}} - \frac{\sigma_{ij}^{6}}{R_{ij}^{6}} \right) \right] \end{aligned} \quad (1)$$

which includes the bond stretching, angle bending, torsional rotation, and nonbonded interaction terms, i.e., a Coulomb term for the charge-charge interactions and a Lennard-Jones 12-6 term for the van der Waals repulsion and dispersion interaction. Here, k_r, k_θ represent the force constants of bond stretching, angle bending, and v_1, v_2, v_3 represent the force constants of dihedral angle torsion, respectively. r_{eq} and θ_{eq} are used to denote the equilibrium values of the bond length and bond angle; r, θ, and ϕ stand for the actual values of bonds, angles, and dihedral angles, respectively. Geometric combining rules for the Lennard–Jones coefficients are employed: $\sigma_{ij} = (\sigma_{ii}\sigma_{jj})^{1/2}$ and $\varepsilon_{ij} = (\varepsilon_{ii}\varepsilon_{jj})^{1/2}$. Furthermore, the coefficient f_{ij} is set to 0.0 for any i–j pair separated by one or two bonds, $f_{ij} = 0.5$ for 1,4 interactions (atoms separated by exactly three bonds) and $f_{ij} = 1.0$ for all of the other cases. For the Coulomb term, the partial charges q_i are obtained by ABEEM model [53, 54], which makes a full consideration on the conformational changes and gives the explicitly quantitative charges of all molecular regions, including atoms, bonds, and lone pairs. R_{ij} is the distance between the site points i and j, k_{ij} is equal to 0.57, which is an overall optimized correction coefficient. In the hydrogen bond interaction region [57, 58], k_{ij} is replaced by a $k_{\text{H-bond}}(R_{ij})$ function to describe the electrostatic interaction between the hydrogen atom and the lone pair electrons.

Figure 2 depicts the atom and lone pair electron charge sites of DMP anion by the ABEEM model. There are totally 35 sites including 13 atoms, 12 bonds, and 10 lone pairs. It provides a more delicate consideration of the electrostatic interaction. In Fig. 2, O1* and O2* are nonesterified oxygen atoms, and O1 and O2 are esterified oxygen atoms. Correspondingly, the lone pairs located in the DMP anion can be classified into two classes: (1) the nonesterified oxygen lone pairs located on the O1* and O2* atoms; (2) the esterified oxygen lone pairs located on the O1 and O2 atoms. The presence of multiple lone pairs leads to additional contributions to the anomeric effect, especially involving the nonesterified oxygen (O*) lone pairs [14]. The charge center of lone pair is placed on the point that is covalent atomic radius far from the bonded atomic nucleus. The bond charge is located on the point

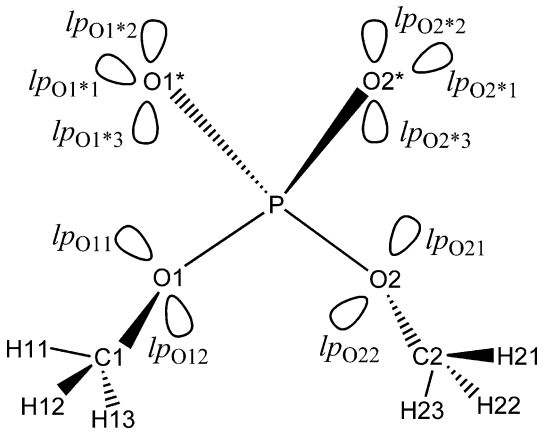

Fig. 2 Atom and lone pair charge sites of DMP anion assigned by the ABEEM model. The nonesterified oxygen atoms are denoted as O1* and O2*, and the esterified oxygen atoms are denoted as O1 and O2. '*lp*' represents lone pair. For example, 'lp_{O1*1}' denotes the first lone pair of O1*. In the text the nonesterified oxygen atoms are frequently referred together as O* and the esterified oxygen atoms as O

that partitions the bond length according to the ratio of covalent atomic radii of two bonded atoms.

It is very important to include the effects of hydrogen bonding in molecular simulation based on classical force fields if one hopes to reproduce and explain a wide range of chemical phenomena. As there are two types of lone pairs, we considered two types of hydrogen bonds between DMP anion and water molecule. The first one is the hydrogen bond forming between the lone pair of nonesterified oxygen and the hydrogen of water molecule (i.e. *lp*O*···Hw); the second one is the hydrogen bond forming between the lone pair of esterified oxygen and the hydrogen of water molecule (i.e. *lp*O···Hw). In order to well depict the nature of the two types of hydrogen bonds, we take the special treatments by introducing the parameters $k_{lpO^*\cdots Hw}(R_{lpO^*\cdots Hw})$ and $k_{lpO\cdots Hw}(R_{lpO\cdots Hw})$ to describe the electrostatic interactions of the two types of hydrogen bonds. The fitted expressions of $k_{lpO^*\cdots Hw}(R_{lpO^*\cdots Hw})$ and $k_{lpO\cdots Hw}(R_{lpO\cdots Hw})$ are expressed as follows:

$$k(R_{lpO^*\cdots Hw}) = 0.630 - \frac{0.1086}{1+\exp[(R_{lpO^*\cdots Hw}-1.286)/0.1910]} \quad (2)$$

$$k(R_{lpO\cdots Hw}) = 0.603 - \frac{0.0683}{1+\exp[(R_{lpO\cdots Hw}-2.085)/0.0862]} \quad (3)$$

Minimizations of isolated DMP anion and DMP-water clusters were performed using the modified Tinker 4.2 program with the limited memory BFGS quasi-Newton nonlinear optimization routine. The criterion used for convergence was the root-mean-square energy gradient, which was less than 0.01 kcal/mol/Å. No restrictions were applied, that is, all atoms are allowed to move freely. By the way, the original orientations were identical to those used in the QM calculations.

A classical molecular dynamics (MD) simulation was performed in terms of the ABEEM/MM and AMBER ff99, respectively, starting with a DMP anion in gg conformation and a sodium counterion (Na^+ was placed arbitrarily) in a cubic box of length 18.64 Å containing 220 preequilibrated H_2O molecules. The system was optimized first, and then the MD simulation was carried out in a canonical ensemble, with periodic boundary condition and the minimum image convention. Temperature was kept constantly at 300 K by Berendsen algorithm. The equations of motion were solved using the velocity Verlet algorithm with a time step of 1 fs. The long-range interactions were truncated using a molecule based cutoff distance of 9.0 Å. The system was equilibrated within 500 ps, and the following 500 ps trajectory was collected for dynamical property analysis. It should be mentioned that, during the ABEEM/MM MD, the charges of atoms, bonds, and lone pairs were recalculated every picosecond instead of each time step.

Quantum mechanical calculations were performed by using the Gaussian 03 program package [66]. Geometries were determined at the DFT level by means of B3LYP nonlocal exchange-correlation functional [67, 68] with 6-311++G** basis set. Calculations of vibrational frequencies were performed to confirm that the optimized structures were at their energy minima. Energies were determined within the Møller-Plesset perturbation method (MP2) [69] with the same basis set, and BSSE corrections [70] were included for $DMP(H_2O)_n$ ($n = 1$–3) clusters. All the calculations were performed on an SGI Altix 3700 server with 64 Itanium CPUs.

3 Results and discussion

3.1 Properties of isolated DMP anion

The charge distributions of isolated DMP anions (gg, gt, tt) calculated by the ABEEM model are listed in Table 1 in detail, from which we can see that the charge distributions of gg, gt, and tt are different from each other, especially those of the atoms and lone pairs, which is mainly due to the intramolecular environment changes. For all the three conformations, the positive charges are located on the atoms including phosphorus, nonesterified oxygen, and methylic atoms, and the negative charges are located on the esterified oxygen atoms, all the bonds and lone pairs. The total charge of each DMP anion is −1.

The internal geometries corresponding to the gg, gt, and tt conformations are listed in Table 2, which are obtained

Table 1 Charge distributions for DMP anion by the ABEEM/MM model

Atom	gg	gt	tt	Bond	gg	gt	tt	*lp*	gg	gt	tt
q_{P}	1.405	1.401	1.392	$q_{P–O1*}$	−0.090	−0.090	-0.090	q_{lpO1*1}	−0.266	−0.257	−0.264
q_{O1*}	0.126	0.126	0.125	$q_{P–O2*}$	−0.090	−0.091	−0.090	q_{lpO1*2}	−0.261	−0.260	−0.266
q_{O2*}	0.126	0.126	0.125	q_{P-O1}	−0.079	−0.078	−0.077	q_{lpO1*3}	−0.266	−0.267	−0.270
q_{O1}	−0.022	−0.021	−0.021	$q_{P–O2}$	−0.079	−0.078	−0.077	q_{lpO2*1}	−0.266	−0.272	−0.264
q_{O2}	−0.022	−0.022	−0.021	$q_{O1–C1}$	−0.085	−0.085	−0.085	q_{lpO2*2}	−0.261	−0.270	−0.266
q_{C1}	0.117	0.119	0.117	$q_{O2–C2}$	−0.085	−0.085	–0.085	q_{lpO2*3}	−0.266	−0.266	−0.270
q_{C2}	0.117	0.115	0.117	$q_{C1–H11}$	−0.100	−0.100	−0.100	q_{lpO11}	−0.186	−0.186	−0.184
q_{H11}	0.097	0.103	0.098	$q_{C1–H12}$	−0.101	−0.100	−0.100	q_{lpO12}	−0.190	−0.182	−0.180
q_{H12}	0.100	0.098	0.104	$q_{C1–H13}$	−0.100	−0.100	−0.101	q_{lpO21}	−0.186	−0.189	−0.184
q_{H13}	0.103	0.102	0.098	$q_{C2–H21}$	−0.100	−0.101	−0.100	q_{lpO22}	−0.190	−0.185	−0.180
q_{H21}	0.097	0.098	0.098	$q_{C2–H22}$	−0.100	−0.100	−0.101				
q_{H22}	0.103	0.097	0.098	$q_{C2–H23}$	−0.101	−0.101	−0.100				
q_{H23}	0.100	0.101	0.104								

All calculated charges in au

Table 2 Comparison of the geometries of DMP anion

	gg			gt		tt	
	ABEEM	DFT[a]	Exp[b]	ABEEM	DFT[a]	ABEEM	DFT[a]
Bond length							
P–O1*	1.498	1.498		1.497	1.495	1.499	1.504
P–O2*	1.498	1.498		1.501	1.507	1.499	1.504
P–O1	1.623	1.680		1.619	1.661	1.630	1.672
P–O2	1.623	1.680		1.631	1.688	1.630	1.672
O1–C1	1.420	1.417		1.420	1.418	1.423	1.415
O2–C2	1.420	1.417		1.421	1.414	1.423	1.415
C1–C2	3.962	3.955		4.276	4.263	5.036	5.024
Bond angle							
O1*–P–O2*	121.5	125.7	119.7	120.7	123.4	120.4	122.4
O1–P–O2	101.7	99.5	104.8	98.5	96.1	97.2	95.0
P–O1–C1	119.9	117.9	121.7	119.9	118.5	120.6	118.4
P–O2–C2	119.9	117.9	121.7	120.2	117.2	120.6	118.4
Torsional angle							
C1–O1–P–O2	73.8	74.2	73	69.2	70.2	141.7	142.2
O1–P–O2–C2	73.8	74.2	73	−163.5	−164.2	141.7	142.2
O1*–P–O2*–C1	125.1	126.4		126.5	127.8	127.8	129.2
O1*–P–O2*–C2	−125.7	−127.6		−127.4	−128.9	−127.1	−128.4

Bond lengths in angstrom. Angles in degree. For atomic numbering, see Fig. 2

[a] DFT calculations at B3LYP/6-311++G** level

[b] Experimental values from Ref. [71]

from the ABEEM/MM model and QM calculations at B3LYP/6-311++G** level, along with the experimental data [71] for the gg conformation. Comparison of the structures for bond lengths, angles, and torsional angles shows satisfactory agreement between the ABEEM/MM results and the B3LYP/6-311++G** level calculations. For bond length, the RMSD is 0.027 Å, and the most obvious discrepancy occurs to the P–O bonds. For instance, the bond length of P–O in gg conformation from ABEEM/MM model is 1.623 Å versus the value of 1.680 Å from B3LYP calculations. However, the P–O bonds in crystal structure of barium diethyl phosphate are 1.59 and 1.62 Å [9]. So the shorter ABEEM/MM bond length is more adequate to reproduce the condensed phase properties. The

RMSD of angles is 2.4°, the biggest discrepancy occurs to the O*–P–O* angle of gg conformation with difference of 4.2°. The experimental value of the O*–P–O* angle obtained by X-ray diffraction is 119.7°. We can see that, the ABEEM/MM value (121.5°) is closer to the experimental data than the B3LYP result (125.7°). The RMSD of torsional angles between ABEEM/MM and B3LYP results is merely 1.1°, which is also acceptable. Furthermore, the torsional angle of 73.8° for C–O–P–O of gg conformation from ABEEM/MM model is in good agreement with experimental result (73°).

It is well known that the gg conformation is more stable than the gt, and tt conformations due to the conventional anomeric effect. Proper energy ordering of the three gas phase conformations (gg, gt, and tt) is essential for simulating DMP anion. Table 3 listed the conformational energies of these three conformations by using the present ABEEM/MM model, AMBER force field [27], and several ab initio methods [9, 14, 18]. The common point among all the methods is the energy order of gg, gt, and tt configurations, i.e., the gg conformation has the lowest energy in the gas phase, followed by the gt and tt conformations. The gt conformation is 1.11 kcal/mol higher than the gg geometry, and the tt is 3.32 kcal/mol from the ABEEM/MM model. The conformational energies obtained by MP2/6-311++G** level ab initio calculations for gt and tt conformations are 1.14 and 3.35 kcal/mol, respectively. Agreements between the ABEEM/MM force field results and the ab initio calculations concerning both the order and relative energy differences of the conformations are quite well. The calculated gg/gt and gg/tt energy difference is 1.42 and 2.83 kcal/mol from earlier AMBER force field [27]. Obviously, the ABEEM/MM results are in better agreement with the ab initio data.

Table 3 Comparison of relative energies for DMP anions

DMP	gg	gg–gt	gt	gt–tt	tt
ABEEM/MM	0.00	2.41	1.11	4.20	3.32
MP2/6-311++G**// B3LYP/6-311++G**	0.00	1.91	1.14	3.39	3.35
MP2/6-31+G*//HF/6-31G*[a]	0.00	2.26	1.45		3.66
B3LYP/6-31G**// B3LYP/6-31G**[b]	0.00		0.98		
MP2/6-31+G*// MP2/6-31+G*[c]	0.00		1.37		3.34
AMBER[d]	0.00		1.42		2.83

All calculated energies in kcal/mol

[a] Ref. [9]

[b] Ref. [18]

[c] Ref. [14]

[d] Ref. [27]

As shown in Table 3, the torsional barriers going from gg to gt and from gt to tt were also computed at MP2/6-311++G**//B3LYP/6-311++G** level, as well as the ABEEM/MM method. The conformational transition from gt to tt is less favorable than that of gg to gt, due to the higher energy barrier of gt to tt. The ABEEM/MM torsional barriers going from gg to gt to tt for DMP in the gas phase are a little higher (less than 1.0 kcal/mol) than the corresponding ab initio results.

3.2 Properties of $DMP(H_2O)_n$ ($n = 1$–3) clusters

Water is a basic and integral part of nucleic acid structure. Interactions with water molecules are important for the stabilization of three-dimensional structures of nucleic acids and for their functioning, such as double helix formation in DNA or chain folding in RNA. Even under extremely dehydrating conditions, nucleic acids still have some tightly associated water [72]. Previous QM calculations suggested that water molecules play an important role in the conformational flexibility of DMP anion [73]. Here, we studied 11 $DMP(H_2O)_n$ ($n = 1$–3) complexes, in which the gg conformation is adopted for the DMP anion.

The calculated equilibrium geometries (such as H-bond lengths and H-bond angles) of DMP-H_2O dimers are shown in Fig. 3. The ABEEM/MM optimized H-bond lengths (Å) and H-bond angles (°) are shown first, followed by B3LYP/6-311++G** values in parentheses. There are mainly two possible positions (I and II) for forming hydrogen bonds around DMP anion: (1) One water molecule lies close to the O*–P–O* plane at position I. Two O*···Hw–Ow type hydrogen bonds are formed. We call this complex DMP1-1, which is shown in Fig. 3 (left). A six-member-ring in DMP1-1 is clearly seen; (2) One water molecule interacts with one O and one O* at position II shown in Fig. 3 (right), and the complex is called DMP1-2. There are two kinds of H-bonds in DMP1-2: the first one (O*···Hw–Ow) is similar to that of DMP1-1, but the H-bond length becomes shorter and the angle becomes linear, which indicates that the H-bond of O*-Hw-Ow in DMP1-2 is stronger than that in DMP1-1; the second one is formed between the esterified oxygen atom (O) and Hw, and it has the longest H-bond length and the smallest angle, which shows that it is the weakest.

As mentioned above, two types of H-bonds (O*···Hw–Ow and O···Hw–Ow) are found due to the difference of nonesterified (O*) and esterified (O) oxygen atoms. With respect to the equilibrium geometry values for H-bond lengths and H-bond angles in DMP-H_2O dimer, the RMSD between the ABEEM/MM and B3LYP results are 0.020 Å and 1.2°, respectively. The ABEEM/MM results are in exceptional accordance with the corresponding DFT results. The ABEEM/MM equilibrium geometry for bond

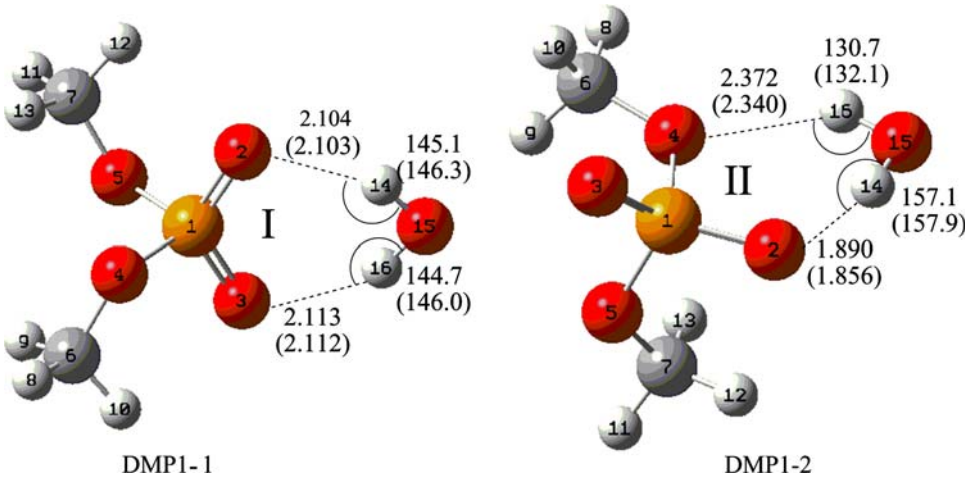

Fig. 3 Structures of DMP-H_2O dimer. The ABEEM/MM optimized H-bond lengths (Å) and H-bond angles (°) are shown firstly, followed by the B3LYP/6-311++G** values in parentheses

Table 4 Charge distributions for DMP-H_2O dimers by the ABEEM/MM model

Atom	DMP1-1	DMP1-2	Bond	DMP1-1	DMP1-2	*lp*	DMP1-1	DMP1-2
q_P	1.415	1.413	$q_{P–O1*}$	−0.090	−0.089	q_{lpO1*1}	−0.254	−0.294
q_{O1*}	0.113	0.109	$q_{P–O2*}$	−0.090	−0.090	q_{lpO1*2}	−0.275	−0.283
q_{O2*}	0.113	0.127	$q_{P–O1}$	−0.079	−0.079	q_{lpO1*3}	−0.279	−0.253
q_{O1}	−0.022	−0.023	$q_{P–O2}$	−0.079	−0.079	q_{lpO2*1}	−0.254	−0.262
q_{O2}	−0.022	−0.022	$q_{O1–C1}$	−0.085	−0.085	q_{lpO2*2}	−0.274	−0.256
q_{C1}	0.122	0.121	$q_{O2–C2}$	−0.085	−0.085	q_{lpO2*3}	−0.279	−0.261
q_{C2}	0.122	0.122	$q_{C1–H11}$	−0.100	−0.100	q_{lpO11}	−0.183	−0.189
q_{H11}	0.101	0.101	$q_{C1–H12}$	−0.100	−0.100	q_{lpO12}	−0.187	−0.193
q_{H12}	0.103	0.102	$q_{C1–H13}$	−0.100	−0.100	q_{lpO21}	−0.183	−0.183
q_{H13}	0.106	0.106	$q_{C2–H21}$	−0.100	−0.100	q_{lpO22}	−0.187	−0.187
q_{H21}	0.101	0.101	$q_{C2–H22}$	−0.100	−0.100	q_{lpOw1}	−0.242	−0.236
q_{H22}	0.106	0.107	$q_{C2–H23}$	−0.100	−0.100	q_{lpOw2}	−0.242	−0.237
q_{H23}	0.103	0.103	$q_{Ow–Hw1}$	−0.151	−0.146			
q_{Ow}	0.103	0.102	$q_{Ow–Hw2}$	−0.151	−0.152			
q_{Hw1}	0.342	0.419						
q_{Hw2}	0.340	0.251						

All calculated charges in au, for numbering, see Fig. 2

lengths of O*···Hw–Ow and O···Hw–Ow are systemic longer than those of the B3LYP calculations by 0.001–0.034 Å; in contrast, the values of angle O*···Hw–Ow and angle O···Hw–Ow are a bit smaller by 0.8–1.4°.

The charge distributions of DMP-H_2O dimers are listed in Table 4. For the water molecule, ABEEM-7P model [57, 58] gives the explicitly quantitative charges of all atoms, bonds, and lone pairs. The positive charges located on the Ow atom (0.113) and Hw atoms (0.290) are balanced by the negative charges located on the Ow–Hw bonds (−0.155) and the lone pairs (−0.191). As seen from data in Tables 1 and 4, the charges of all sites for each DMP-water dimers are different from the isolated water and DMP anion, which is consequential upon the environmental changes. The remarkable change of charges takes place at the position where the hydrogen bond forms. For example, obvious polarization takes place for the charges of Hw1, Hw2, *lp*O1*2, *lp*O1*3, *lp*O2*2, and *lp*O2*3 in complex DMP1-1 (See Fig. 2 for notation of charge sites of DMP anion), i.e., *q*Hw1 and *q*Hw2 are 0.342 and 0.340 versus 0.290 in isolated water hydrogen, and the charges of *lp*O1*2 (−0.275), *lp*O1*3 (−0.279), *lp*O2*2 (−0.274), and *lp*O2*3 (−0.279) are more negative than those of the isolated DMP anion (−0.261, −0.266, −0.261, and −0.266), respectively. In the same way, this obvious polarization also takes place for complex DMP1-2 for the charges of Hw1, Hw2, *lp*O1*1, *lp*O1*2, *lp*O11, and *lp*O12. In addition, we can predict the orientation of the water molecules interacting with DMP anion by the charge distributions. For example, the water hydrogen atoms have more positive

charge and the lone pairs of O1* and O2* have more negative charge in complex DMP1-1, which means that two water hydrogen atoms will interact with both non-esterified oxygen atoms of DMP anion at position I, respectively. Compared with the isolated water and DMP anion, in complex DMP1-2, the charges of Hw1, Hw2 and lone pairs of O1* and O1 change obviously, which means that there are hydrogen bonds at position II. To summarize, the fluctuating charges of the DMP anion and water molecule can correctly reflect the redistribution with the changed ambient environment and provide insight into the intermolecular interaction of the system.

In order to further examine whether the ABEEM/MM potential model can reproduce the ab initio interaction energies, the interaction energies ΔE of $DMP(H_2O)_n$ ($n = 1$–3) clusters are calculated and compared with the quantum chemical results. The interaction energy ΔE is defined as the difference between the total energy of a complex and the sum of each separated molecules. Eleven complexes have been studied here: DMP1-1 and DMP1-2 are DMP-H_2O dimers as describing above; DMP2-1, DMP2-2, DMP2-3, and DMP2-4, are $DMP(H_2O)_2$ trimers; five $DMP(H_2O)_3$ clusters are studied, i.e., DMP3-1, DMP3-2, DMP3-3, DMP3-4, and DMP3-5. The geometric structures of the complexes of $DMP(H_2O)_n$ ($n = 2$, 3) are shown in Fig. 4. For all the complexes, there are mainly two types of hydrogen bonds between DMP anion and water molecule. And the hydrogen bonds between two water molecules cannot be neglected. The interaction energies of $DMP(H_2O)_n$ ($n = 1$–3) clusters calculated at the MP2/6-311++G**//B3LYP/6-311++G** level with BSSE corrections are listed in Table 5. For DMP-H_2O dimers, the interaction energy of DMP1-1 (−14.57 kcal/mol) is a little lower than DMP1-2 (−14.45 kcal/mol). In the case of $DMP(H_2O)_2$ clusters, two water molecules attached to the DMP anion as two water monomers (DMP2-1 and DMP2-2) or a water dimer (DMP2-3 and DMP 2-4), and the energy differences between them are fairly small, with the interaction energies varied from −26.87 to −27.90 kcal/mol. For the $DMP(H_2O)_3$ clusters, almost the same interaction energies are obtained.

Table 5 also lists the interaction energy of $DMP(H_2O)_n$ ($n = 1$–3) calculated by the ABEEM/MM model, which are found to be in good agreement with the foregoing QM calculations with an RMSD of 0.87 kcal/mol. The largest discrepancy occurs at the DMP3-4 complex, and the difference is −1.94 kcal/mol, which is less than 5% of the interaction energy. On the other hand, the order of $DMP(H2O)_n$ ($n = 1$, 2) is in good agreement with the ab initio calculations, with the only exception of DMP2-2, which is 1.29 kcal/mol higher than the QM result (−27.90 kcal/mol). In the cases of $DMP(H_2O)_3$, we failed

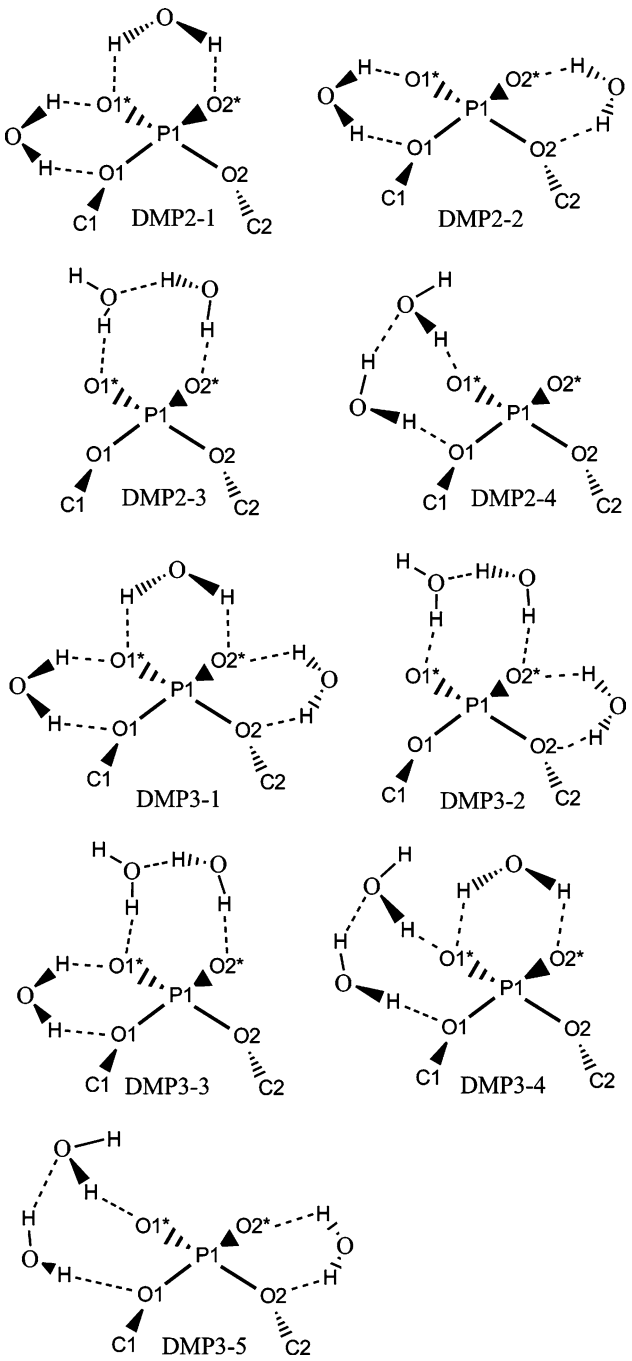

Fig. 4 Graphical representation of the $DMP(H_2O)_n$ ($n = 2$, 3) clusters

in calculating the order of interaction energies, due to the small energy differences between the five complexes. In a word, the differences of stabilization energy of $DMP(H_2O)_n$ complexes are acceptable, and we can draw a conclusion from the above analysis that the ABEEM/MM model can well give rise to and correctly calculate the static properties of $DMP(H_2O)_n$ complexes, and compare well with the ab initio calculations.

Table 5 Interaction energies of DMP-$(H_2O)_n$ (n = 1–3) clusters

	ABEEM/MM	Ab initio[a]	Deviation
DMP1-1	−14.51	−14.57	0.06
DMP1-2	−13.77	−14.45	0.68
DMP2-1	−27.74	−27.76	0.02
DMP2-2	−26.61	−27.90	1.29
DMP2-3	−27.20	−27.13	−0.07
DMP2-4	−26.88	−26.87	−0.01
DMP3-1	−39.98	−39.98	0.00
DMP3-2	−41.08	−39.56	−1.52
DMP3-3	−39.51	−39.56	0.05
DMP3-4	−41.47	−39.53	−1.94
DMP3-5	−39.31	−39.69	0.38

All energies in kcal/mol

[a] Ab initio calculations at the MP2/6-311++G**//B3LYP/6-311++G** level with BSSE corrections

3.3 MD simulation of DMP anion in aqueous solution

In order to further test and verify the reasonableness of the ABEEM/MM model and the correctness and transferability of the parameters, we performed a MD simulation of DMP anion in aqueous solution. The results are compared with AMBER ff99, CHARMM22, and ab initio MD simulations [15]. Qualities such as the radial and angular distributions of water around the nonesterified oxygen atoms (O*) in DMP anion are reported.

3.3.1 Geometries of the DMP anion in gas phase and aqueous solution

The averaged geometry parameters of DMP anion obtained by ABEEM/MM, AMBER ff99, CHARMM22 and ab initio MD simulations are listed in Table 6. The standard deviations are given in parentheses. The small deviations for bond lengths (about 0.03 Å) and angles (about 2°) indicate that the present system is equilibrated. As expected, the geometric parameters from ABEEM/MM and AMBER ff99 are quite close to each other. Furthermore, the ABEEM/MM MD simulation results are identical to those obtained previously by Kuo et al. [15] using the ab initio MD and CHARMM22 force field. Comparing the average structure of ABEEM/MM MD simulation with the geometry from the *ab initio* MD shows that the bond lengths are quite similar with differences of 0.03–0.06 Å, and 1–3° differences are observed for angle bending. In addition, the average structure from the ABEEM/MM MD is very close to the crystalline structure listed in Table 2. The optimized geometrical parameters of the DMP anion obtained at MP2/6-31G** level in gas phase and at B3LYP/6-311++G** level in aqueous solution are listed in Table 6. Comparing the average structure from the ABEEM/MM MD simulation with the optimized geometry in gas phase, a 6° opening of the O1–P–O2 angle and a 7° closing of the O1*–P–O2* angle are observed, which indicate that there are small but significant solvent effects on the phosphate geometry.

3.3.2 Radial distribution

Besides the geometrical changes of DMP anion, the arrangement of water around the DMP anion is remarkably varied, with the most interesting results appearing in the highly ionic regions between the nonesterified oxygen atoms in DMP anion [74]. Radial distribution function (RDF) is a useful tool to describe the structure of a system, particularly of liquids, and the peaks of the RDF can reflect the shell structure of the solvent. Here, the structure feature of the water molecules surrounding the DMP anion is

Table 6 Geometric parameters for the DMP anion from molecular dynamics simulations in aqueous solution and geometry optimizations

Geometry	AI MD[a]	ABEEM/MM	AMBER	CHARMM[a]	AI opt[a] (gas)	DFT opt[b] (aqueous)
P–O1*	1.52 (0.02)	1.48 (0.03)	1.48 (0.02)	1.48 (0.02)	1.50	1.51
P–O2*	1.52 (0.02)	1.48 (0.02)	1.48 (0.02)	1.48 (0.02)	1.50	1.51
P–O1	1.63 (0.03)	1.60 (0.03)	1.60 (0.03)	1.58 (0.03)	1.68	1.65
P–O2	1.63 (0.03)	1.60 (0.03)	1.60 (0.03)	1.58 (0.03)	1.68	1.65
O1–C1	1.48 (0.04)	1.42 (0.03)	1.42 (0.03)	1.43 (0.03)	1.42	1.43
O2–C2	1.48 (0.04)	1.42 (0.03)	1.42 (0.03)	1.43 (0.03)	1.42	1.43
O1–P–O2	104 (4)	105 (2)	105 (4)	103 (3)	99	102
O1–P–O2*	107 (5)	108 (2)	108 (3)	109 (3)	106	105
O2–P–O1*	105 (4)	109 (2)	108 (3)	109 (3)	106	105
O1*–P–O2*	117 (3)	119 (2)	119 (3)	116 (3)	126	122

Bond lengths in angstrom. Angles in degree. MD results are average values, with the standard deviations given in parentheses

[a] Ref. [15]

[b] DFT optimization at B3LYP/6-311++G** level with continuum model

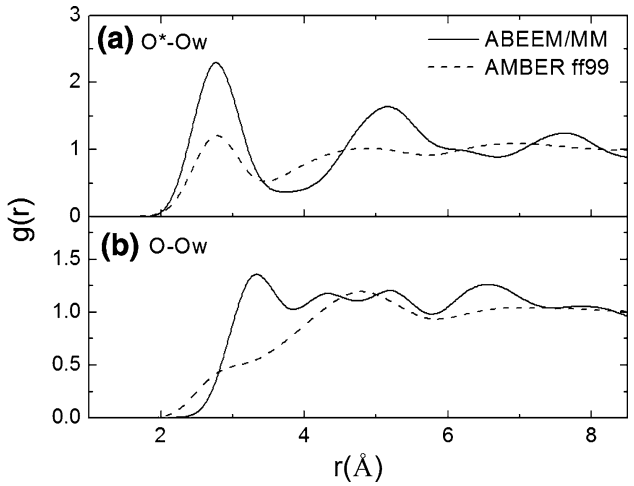

Fig. 5 Radial distribution function for water oxygen atoms around the nonesterified (**a**) and esterified (**b**) oxygen atoms of a DMP anion from the ABEEM/MM (*solid line*) and AMBER ff99 (*dashed*) MD simulations

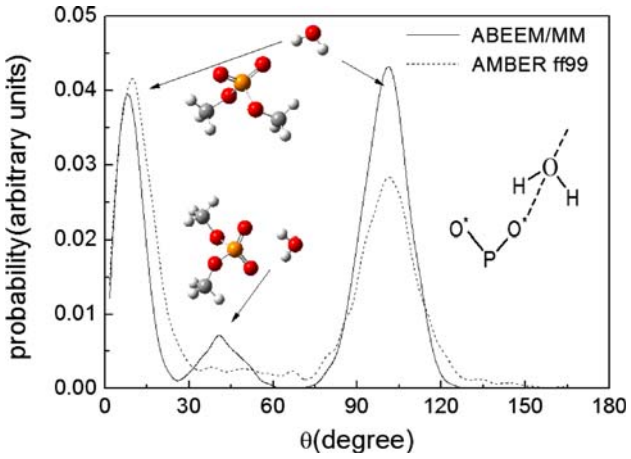

Fig. 6 Orientational probability distributions for water molecules within the first hydration shell of the nonesterified oxygen atoms of a DMP anion from the ABEEM/MM (*solid line*) and AMBER ff99 (*dashed*) MD simulations

described by the RDF of the Ow atoms around the nonesterified (Fig. 5a) and esterified (Fig. 5b) oxygen atoms. The well-pronounced feature of the ABEEM/MM O*···Ow RDF (solid line) is a sharp peak corresponding to the first hydration shell, followed by a lower and broader second peak. The third peak is very weak. It implies that the DMP anion can influence about two solvation shells from the ABEEM/MM MD simulation. The water becomes fully bulk like at the third solvation shell at about 7.5 Å distance. The sharp first peak with a maximum at 2.75 Å marks a tight first hydration shell of the O* atoms in DMP anion, which is shifted outward about 0.05 Å when comparing to the ab initio simulation (2.7 Å) [15]. The average coordination number of the two O* atoms within the first hydration shell determined by integration of the first peak in the RDF is 5.2, which is close to 5.0 and 5.5 from ab initio and CHARMM MD simulations [15]. However, the first peak is shorter and there is no evident second peak in the O*···Ow RDF (dashed) from the AMBER simulation. For the esterified oxygen atoms, the RDF of O–Ow do not show a clear structure in both curves. We believe that the stronger interaction of O*–Ow in the ABEEM/MM curve is a consequence of the multi *lp*O* charge sites (see Fig. 2), which have more negative charge than *lp*O. In addition, the methyl connecting to the esterified O atom could block the water molecules binding to the esterified oxygen atoms.

3.3.3 Angular distribution

To quantify the orientation of water molecules in the vicinity of the phosphate group, we used θ as the angle between the Ow–O* vector and the Ow–Hw vector. The angular distribution calculated up to the first minimum in the O*–Ow RDF gives some insight into the overall arrangement of the water molecules around the DMP anion in aqueous solution. The probability distributions of angle θ from ABEEM/MM (solid line) and AMBER ff99 (dashed) are plotted in Fig. 6. For the ABEEM/MM curve, the first sharp peak at $\theta = 8°$ arises from tightly bound water molecules within the first hydration shell pointing one of the Hw toward a nonesterified O* oxygen atom of DMP anion in a nearly linear hydrogen bond. The second sharp peak at θ = 101° corresponds to the hydrogen atoms of water molecules that do not form hydrogen bonds with the DMP anion. There are two sharp peaks at 9 and 100° from the AMBER MD simulation. These two sharp peaks reveal the most populated type of DMP-water interactions in DMP solution, i.e., the two hydrogen atoms of a water molecule do not simultaneously interacting with an O* atom in DMP anion (as shown in the upside of Fig. 6).

At a glance of Fig. 6, it is obvious to see a short peak located at about $\theta = 40°$ in the ABEEM/MM curve, which is the biggest difference between ABEEM/MM and fixed charge force fields or ab initio MD simulations. This peak arises from a particular case that two hydrogen atoms of one water molecule form two hydrogen bonds with two O* of the DMP anion simultaneously, corresponding to the interaction mode of water with DMP anion at position I as shown in Fig. 3 (left) and Fig. 6 (underside). It is reasonable and important due to the lower interaction energy of DMP1-1 (Fig. 3). The reason why the probability of this interaction mode is smaller lies in two aspects: (1) The space between two O* (region I in Fig. 3), accommodating one water molecule to form two H-bonds with the DMP anion is relatively small. (2) The energy difference between the two interaction modes observed in the angular

distribution curve is not very big (about several kcal/mol), and it can be easily overcome by the intermolecular collisions at the room temperature. So the interaction mode of the lowest interaction energy can convert to another interaction mode of higher interaction energy.

All in all, it is clear that the obtained statistically averaged solvation shell is different between ABEEM/MM and AMBER MD simulations. There is a shorter first solvation shell and no evident second solvation shell when the standard AMBER ff99 force field is used, but the first and second hydration shells of DMP anion are very well defined around the nonesterified O* atoms from the ABEEM/MM MD simulation. Furthermore, the energy advantaged interaction mode in DMP-water cluster (DMP1-1) was only found in the ABEEM/MM MD simulation. From the above analyses, we concluded that using the environment-dependent atomic charge model is reasonable and important for the simulation of DMP system.

4 Conclusion

This work presents potential energy function and parameters for DMP systems based on the ABEEM/MM fluctuating charge model. The essence of this potential model is to take the ABEEM charges of all atoms, bonds, and lone pairs of DMP anion and water molecules into the electrostatic interaction term in molecular mechanics. Here, the DMP anion is modeled by 35 charge sites, including 13 atoms, 12 bonds, and 10 lone pairs, and it provides a more delicate consideration for DMP anion in the electrostatic interaction. The model has the following characters: (1) it allows the charges in system to fluctuate corresponding to the ambient environment; (2) special treatments are taken for intermolecular hydrogen bonds in describing the electrostatic interaction by the use of function $k_{\text{H-bond}}(R_{ij})$.

In the present paper, we systemically investigated the geometry and energy properties of isolated DMP anion and DMP-water complexes based on the ab initio method and ABEEM/MM fluctuating charge model. The ABEEM/MM conformational energies and geometries of three DMP minima are in good agreement with the QM calculations or available experimental data. Studies of the DMP-$(H_2O)_n$ ($n = 1$–3) clusters further indicate that the present model is adequate in treating hydrogen bonds in the DMP-water complexes. MD simulation of DMP anion in aqueous solution with explicit water molecules was performed in terms of the present new potential function and parameters. Some properties are in good agreement with the previous ab initio MD simulation. There are small but significant solvent effects on the DMP anion geometry. We verified that the ABEEM/MM based MD simulation observed a structured and oriented first hydration shell around the nonesterified oxygen atoms of DMP anion. The average coordination number of the two O* atoms within the first hydration shall is 5.2. A special case that the two Hw belongs to one water molecule could form two hydrogen bonds with two nonesterified oxygen atoms of DMP anion at the same time is found. This is the biggest difference between ABEEM/MM and AMBER ff99 MD simulations, and this also shows that a fluctuating charge force field can provide more informative results than the conventional fixed charge force fields. In a word, the ABEEM/MM fluctuating charge model can reasonably simulate the phosphate groups, and this work could be used as a starting point in developing a new ABEEM/MM nucleic acid force field.

Acknowledgments We are very grateful to the editor and reviewers' nice suggestions on the manuscript. We also greatly thank Professor Jay William Ponder for providing the Tinker programs. This work was supported by the grant from the National Natural Science Foundation of China (No. 20633050, 20703022 and 20873055), and the Department of Education of Liaoning Province (No. 2007T091, 20060494, and LNET RC0503). Supporting Information Available: The ABEEM/MM fluctuating charge model and parameters for DMP anion are included in the Appendix.

References

1. Guan Y, Wurrey CJ, Thomas GJ Jr (1994) Biophys J 66:225–235. doi:10.1016/S0006-3495(94)80767-2
2. Guan Y, Choy GS-C, Glaser R, Thomas GJ Jr (1995) J Phys Chem 99:12054–12062. doi:10.1021/j100031a039
3. Jayaram B, Mezei M, Beveridge DL (1987) J Comput Chem 8:917–942. doi:10.1002/jcc.540080702
4. Jayaram B, Mezei M, Beveridge DL (1988) J Am Chem Soc 110:1691–1694. doi:10.1021/ja00214a005
5. Jayaram B, Ravishanker G, Beveridge DL (1988) J Phys Chem 92:1032–1034. doi:10.1021/j100316a009
6. Liang CX, Ewig CS, Stouch TR, Hagler AT (1993) J Am Chem Soc 115:1537–1545. doi:10.1021/ja00057a046
7. Landin J, Pascher I, Cremer D (1995) J Phys Chem 99:4471–4485. doi:10.1021/j100013a017
8. Kamitakahara A, Hsu CL, Pranata J (1995) J Mol Struct Theochem 334:29–35. doi:10.1016/0166-1280(94)03966-O
9. Florián J, Baumruk V, Štrajbl M, Bednárová L, Štěpánek J (1996) J Phys Chem 100:1559–1568. doi:10.1021/jp9520299
10. Florián J, Štrajbl M, Warshel A (1998) J Am Chem Soc 120:7959–7966. doi:10.1021/ja9710823
11. Pichierri F, Sarai A (1999) J Mol Struct Theochem 460:103–116. doi:10.1016/S0166-1280(98)00309-1
12. Murashov VV, Leszczynski J (1999) J Phys Chem B 103:8391–8397. doi:10.1021/jp9915735
13. Murashov VV, Leszczynski J (2000) J Mol Struct Theochem 529:1–14. doi:10.1016/S0166-1280(00)00524-8
14. Banavali NK, Mackerell AD Jr (2001) J Am Chem Soc 123:6747–6755. doi:10.1021/ja010295w
15. Kuo IF, Tobias DJ (2001) J Phys Chem B 105:5827–5832. doi:10.1021/jp003900a
16. Schwegler E, Galli G, Gygi F (2001) Chem Phys Lett 342:434–440. doi:10.1016/S0009-2614(01)00604-2

17. Petrov AS, Pack GR, Lamm G (2004) J Phys Chem B 108:6072–6081. doi:10.1021/jp037517s
18. Petrov AS, Funseth-Smotzer J, Pack GR (2005) Int J Quantum Chem 102:645–655. doi:10.1002/qua.20442
19. Potoff JJ, Issa Z, Manke CW Jr, Jena BP (2008) Cell Biol Int 32:361–366. doi:10.1016/j.cellbi.2008.03.002
20. Karplus M (2002) Acc Chem Res 35:321–323. doi:10.1021/ar020082r
21. Kollman PA, Massova I, Reyes C, Kuhn B, Huo S, Chong L, Lee M, Lee T, Duan Y, Wang W, Donini O, Cieplak P, Srinivasan J, Case DA, Cheatham TEIII (2000) Acc Chem Res 33:889–897. doi:10.1021/ar000033j
22. Giudice E, Lavery R (2002) Acc Chem Res 35:350–357. doi:10.1021/ar010023y
23. Simonson T, Archontis G, Karplus M (2002) Acc Chem Res 35:430–437. doi:10.1021/ar010030m
24. Saiz L, Klein ML (2002) Acc Chem Res 35:482–489. doi:10.1021/ar010167c
25. Mackerell AD Jr, Wiórkiewicz-Kuczera J, Karplus M (1995) J Am Chem Soc 117:11946–11975. doi:10.1021/ja00153a017
26. Foloppe N, Mackerell AD Jr (2000) J Comput Chem 21:86–104. doi:10.1002/(SICI)1096-987X(20000130)21:2<86::AID-JCC2>3.0.CO;2-G
27. Cornell WD, Cieplak P, Bayly CI, Gould IR, Merz KM Jr, Ferguson DM, Spellmeyer DC, Fox T, Caldwell JW, Kollman PA (1995) J Am Chem Soc 117:5179–5197. doi:10.1021/ja00124a002
28. Soares TA, Hünenberger PH, Kastenholz MA, Kräutler V, Lenz T, Lins RD, Oostenbrink C, van Gunsteren WF (2005) J Comput Chem 26:725–737. doi:10.1002/jcc.20193
29. Shaik MS, Devereux M, Popelier PLA (2008) Mol Phys 106:1495–1510. doi:10.1080/00268970802060708
30. van der Spole D, Lindahl E, Hess B, Groenhof G, Mark AE, Berendsen HJC (2005) J Comput Chem 26:1701–1718. doi:10.1002/jcc.20291
31. Aduri R, Psciuk BT, Saro P, Taniga H, Schlegel HB, Santalucia J (2007) J Chem Theory Comput 3:1464–1475. doi:10.1021/ct600329w
32. Jorgensen WL (2007) J Chem Theory Comput 3:1877. doi:10.1021/ct700252g
33. Bret C, Field MJ, Hemmingsen L (2000) Mol Phys 98:751–763. doi:10.1080/002689700162108
34. Xie W, Pu J, MacKerell AD Jr, Gao J (2007) J Chem Theory Comput 3:1878–1889. doi:10.1021/ct700146x
35. Xie W, Gao J (2007) J Chem Theory Comput 3:1890–1900. doi:10.1021/ct700167b
36. Soteras I, Curutchet C, Bidon-Chanal A, Dehez F, Ángyán JG, Orozco M, Chipot C, Luque FJ (2007) J Chem Theory Comput 3:1901–1913. doi:10.1021/ct7001122
37. Dehez F, Ángyán JG, Gutiérrez IS, Luque FJ, Schulten K, Chipot C (2007) J Chem Theory Comput 3:1914–1926. doi:10.1021/ct700156a
38. Nakagawa S, Mark P, Ågren H (2007) J Chem Theory Comput 3:1947–1959. doi:10.1021/ct700132w
39. Marenich AV, Olson RM, Kelly CP, Cramer CJ, Truhlar DG (2007) J Chem Theory Comput 3:2011–2033. doi:10.1021/ct7001418
40. Olson RM, Marenich AV, Cramer CJ, Truhlar DG (2007) J Chem Theory Comput 3:2046–2054. doi:10.1021/ct7001607
41. Marenich AV, Olson RM, Chamberlin AC, Cramer CJ, Truhlar DG (2007) J Chem Theory Comput 3:2055–2067. doi:10.1021/ct7001539
42. Schnieders MJ, Ponder JW (2007) J Chem Theory Comput 3:2083–2097. doi:10.1021/ct7001336
43. Geerke DP, van Gunsteren WF (2007) J Chem Theory Comput 2:2128–2137. doi:10.1021/ct700164k
44. Mennucci B, Cappelli C, Cammi R, Tomasi J (2007) Theor Chem Acc 117:1029–1039. doi:10.1007/s00214-006-0221-2
45. Holt A, Karlström G (2008) J Comput Chem 29:1084–1091. doi:10.1002/jcc.20867
46. Holt A, Karlström G (2008) J Comput Chem 29:1905–1911. doi:10.1002/jcc.20952
47. Holt A, Karlström G (2008) J Comput Chem 29:2033–2038. doi:10.1002/jcc.20976
48. Lussetti E, Pastore G, Smargiassi E (2008) Mol Phys 106:9–21. doi:10.1080/00268970701786361
49. Defusco A, Schofield DP, Jordan KD (2007) Mol Phys 105:2681–2696. doi:10.1080/00268970701620669
50. Plattner N, Bandi T, Doll JD, Freeman DL, Meuwly M (2008) Mol Phys 106:1675–1684. doi:10.1080/00268970802314394
51. Sakharov DV, Lim C (2009) J Comput Chem 30:191–202. doi:10.1002/jcc.21048
52. Yang ZZ, Zhang Q (2006) J Comput Chem 27:1–10. doi:10.1002/jcc.20317
53. Yang ZZ, Wang CS (1997) J Phys Chem A 101:6315–6321. doi:10.1021/jp9711048
54. Wang CS, Yang ZZ (1999) J Chem Phys 110:6189–6197. doi:10.1063/1.478524
55. Yang ZZ, Cui BQ (2007) J Chem Theory Comput 3:1561–1568. doi:10.1021/ct600379n
56. Yang ZZ, Wang CS (2003) J Theor Comput Chem 2:273–299. doi:10.1142/S0219633603000434
57. Yang ZZ, Wu Y, Zhao DX (2004) J Chem Phys 120:2541–2557. doi:10.1063/1.1640345
58. Wu Y, Yang ZZ (2004) J Phys Chem A 108:7563–7576. doi:10.1021/jp0493881
59. Yang ZZ, Li X (2005) J Phys Chem A 109:3517–3520. doi:10.1021/jp051106p
60. Li X, Yang ZZ (2005) J Chem Phys 122:084514. doi:10.1063/1.1853372
61. Li X, Yang ZZ (2005) J Phys Chem A 109:4102–4111. doi:10.1021/jp0458093
62. Li X, Gong LD, Yang ZZ (2008) Sci China Ser B 51:1221–1230. doi:10.1007/s11426-008-0129-x
63. Yang ZZ, Qian P (2006) J Chem Phys 125:064311. doi:10.1063/1.2210940
64. Zhang Q, Yang ZZ (2005) Chem Phys Lett 403:242–247. doi:10.1016/j.cplett.2005.01.011
65. Guan QM, Yang ZZ (2007) J Theor Comput Chem 6:731–746. doi:10.1142/S0219633607003520
66. Frisch MJ, Trucks GW, Schlegel HB, Scuseria GE, Robb MA, Cheeseman JR, Montgomery JAJ, Vreven T, Kudin KN, Burant JC, Millam JM, Iyengar SS, Tomasi J, Barone V, Mennucci B, Cossi M, Scalmani G, Rega N, Petersson GA, Nakatsuji H, Hada M, Ehara M, Toyota K, Fukuda R, Hasegawa J, Ishida M, Nakajima T, Honda Y, Kitao O, Nakai H, Klene M, Li X, Knox JE, Hratchian HP, Cross JB, Bakken V, Adamo C, Jaramillo J, Gomperts R, Stratmann RE, Yazyev O, Austin AJ, Cammi R, Pomelli C, Ochterski JW, Ayala PY, Morokuma K, Voth GA, Salvador P, Dannenberg JJ, Zakrzewski VG, Dapprich S, Daniels AD, Strain MC, Farkas O, Malick DK, Rabuck AD, Raghavachari K, Foresman JB, Ortiz JV, Cui Q, Baboul AG, Clifford S, Cioslowski J, Stefanov BB, Liu G, Liashenko A, Piskorz P, Komaromi I, Martin RL, Fox DJ, Keith T, Al-Laham MA, Peng CY, Nanayakkara A, Challacombe M, Gill PMW, Johnson B, Chen W, Wong MW, Gonzalez C, Pople JA (2004) Gaussian 03. Gaussian, Inc., Wallingford
67. Becke AD (1993) J Chem Phys 98:5648–5652. doi:10.1063/1.464913
68. Lee C, Yang W, Parr RG (1998) Phys Rev B 37:785–789. doi:10.1103/PhysRevB.37.785

69. Møller C, Plesset MS (1934) Phys Rev 46:618–622. doi:10.1103/PhysRev.46.618
70. Boys SF, Bernardi F (1970) Mol Phys 19:553–566. doi:10.1080/00268977000101561
71. Weiner SJ, Kollman PA, Case DA, Singh C, Ghio C, Alagona G, Profeta S Jr, Weiner P (1984) J Am Chem Soc 106:765–784. doi:10.1021/ja00315a051
72. Wolf B, Hanlon S (1975) Biochemistry 14:1661–1670. doi:10.1021/bi00679a018
73. Alber F, Folkers G, Carloni P (1999) J Phys Chem B 103:6121–6126. doi:10.1021/jp9901038
74. Alagona G, Ghio C, Kollman PA (1985) J Am Chem Soc 107:2229–2239. doi:10.1021/ja00294a004